Vol. **131** (2017) *ACTA PHYSICA POLONICA A* No. 1

Special Issue of the 6th International Congress & Exhibition (APMAS2016), Maslak, Istanbul, Turkey, June 1–3, 2016

Micromechanical Investigation of Elastic Properties for Polypropylene Fiber-Matrix Composite

E. Günay*

Gazi University, Engineering Faculty, Mechanical Engineering Department, 06570, Maltepe, Ankara, Turkey

In this study, the mechanical properties of unidirectional fiber composites were determined by using the representative volume element method. The aim of this study was to determine the equivalent elastic constants for the "fiber composite polymer (PPE/PP) thermoplastic material" used in a wide variety of engineering applications. At the first step, the micromechanical model was applied to the polypropylene (PP) fiber-matrix composite, and then the microstructure form of the material was analyzed by finite element method considering "rule of mixture". The symmetry boundary conditions have been applied by using the representative volume elements in 3D finite element models. The SOLID187 mesh element of ANSYS was used for the presentation of the microstructure form of the fiber-matrix composite. The elastic constants obtained in this study were respectively as follows: the longitudinal elastic modulus and the Poisson ratio E_1, ν_{12}, the transverse elastic modulus and the Poisson ratio E_2, ν_{23}. For verification, the numerical results were also compared with the literature.

DOI: 10.12693/APhysPolA.131.143

PACS/topics: 62.23.Pq, 81.05.Qk, 62.20.de, 62.20.dj, 02.70.Dh

1. Introduction

A fiber composite material can be defined as a combination of matrix material, a series of continuous fibers with an interface material which holds together these two groups of materials. Such composite materials are widely used in engineering applications to provide high strength and stiffness. The strength of the fiber composite can vary from 10 to 70% compared to the ratio of fiber volume fraction. There is an additional reinforcement volume limit of about 70vol.% to form a composite [1]. In the screening of the new literature, there are various studies and methods on the effect of volume fraction ratios of elastic constants in the fiber composite materials. Representative volume element (RVE) method was used in general. Bhaskar et al. [2] studied on the finite element (FE) modeling of the polypropylene fiber composite to predict the elastic property of the fiber reinforced plastics (FRP) material. According to this study, the most effective parameter to calculate the equivalent elastic constants of the fiber composite material was defined as the stress transfer mechanism between matrix and fiber under axial loading. In other two studies, stress transfer mechanism from matrix to fiber material by shear stresses was examined in detail by using Cox theory [3, 4]. Houshyar et al. [5] performed the polypropylene fiber-matrix composite modeling by using FE analysis (FEA). According to this study, the ratios of matrix to fiber modulus as well as the interfacial stress in reducing first stage of the interfacial failure and increasing equivalent mechanical properties have been found significant. Sun and Vaidya [6] reported the appropriate boundary conditions for the RVE with various loading conditions. They used fiber reinforced materials for prediction of equivalent composite elastic properties. Hbaieb et al. [7] studied on prediction of stiffness of the composite by using the polymer/clay nanocomposites and compared the results with the Mori–Tanaka (M–T) model.

In this study, the boundary conditions were clarified for the proposed model. Jiang et al. [8] reported that the ratio of surface-to-surface distance of adjacent carbon nanotubes (CNTs) to the CNT diameter plays a key role in improving the overall elastic modulus of the CNT-reinforced composites when the tubes were perfectly aligned, completely separated from other tubes, and ideally bonded with the composite matrix. Alfonso et al. [9] presented a review-research about the computational potentialities of the FEM for the modeling and simulation of composite materials. This review showed that the most studied property was the Young modulus and geometric properties. Houshyar et al. [10] studied on the effect of fiber concentration on mechanical and thermal properties of fiber-reinforced polypropylene composites. In their study, Cox–Krenchel and Haplin–Tsai equations were used to predict tensile modulus of random fiber-reinforced composites. Facca et al. [11] used the micromechanical models available in the short fiber composites from literature to predict the stiffness of some commercially important natural fiber composite formulations. Klasztorny [12] studied on the previous formulations of the exact stiffness theory, and the theory was developed further based on selected boundary-value problems of elasticity theory. In this article, 3D finite element modeling was used to calculate the four elastic constants i.e. E_1, E_2, ν_{12}, ν_{23} of the transversely isotropic PPE/PP fiber composite.

2. Micromechanical modeling

FE modeling with RVE obtained by using 9, 16, 25, 36, and 49 fibers embedded into rectangular and cubic

*e-mail: ezgigunay@gazi.edu.tr

matrix prisms. In this study, $420 \times 420 \times 250$ μm^3 and $420 \times 420 \times 420$ μm^3 dimensions for unit-cell were used. The properties for the matrix material polypropylene co-ethylene (PPE) were $E = 1.05$ GPa, $\nu = 0.33$ and for the PP fiber was $E = 4.5$ GPa, $\nu = 0.2$. In this paper, fibers were arranged parallel to each other with equal spaces between them and it was named as "the transversely isotropic composite". This type of composite defined with five linearly independent elastic constants: E_1, E_2, ν_{12}, ν_{23}, G_{12}. Subscripts 1, 2 and 3 represented the orthogonal coordinate system and also the principle axes of the fiber composite structure. The first axis was named as 1-axis and it was defined along the fiber direction which was parallel to Z axis. The second one named as 2-axis and it was defined with the perpendicular axis to the fiber directions and named as X axis. The third one was named as 3-axis which was perpendicular to the 1–2 plane and which was denoted as Y axis. These three principle axes were denoted by the Z–X–Y axes in the ANSYS solutions, respectively (Figs. 1, 2). For the polypropylene fiber-matrix composites, each of these five volume fractions; V_f(%)=10%, 17%, 27%, 40%, 54% was calculated with four elastic constants E_1, E_2, ν_{12}, ν_{23} (Table I) [2]. The first elastic modulus E_1 was obtained from the cubic matrix with dimensions $420\times420\times420$ μm^3 (Fig. 1) while the second elastic constant was obtained by the rectangular prism with dimensions $420\times420\times250$ μm^3 (Fig. 2).

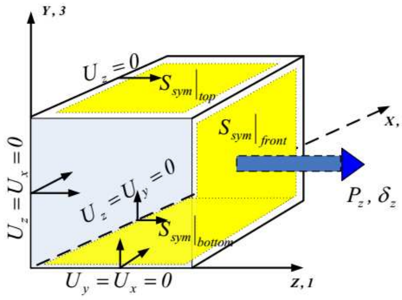

Fig. 1. Boundary conditions for the longitudinal modulus of composite in Z direction (parallel to the fiber direction) E_1.

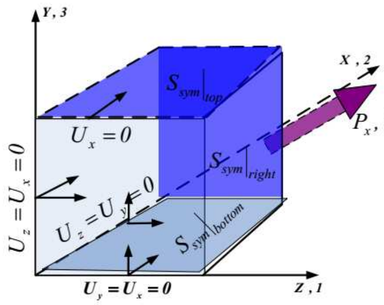

Fig. 2. Boundary conditions for the transverse modulus of composite in X direction (perpendicular to the fiber direction) E_2.

ANSYS13.0 mesh element type was SOLID187 3D ten-node tetrahedral structural solid element with three degrees of freedom per node (U_x, U_y, U_z). In the calculation of the first and second elastic modulus values E_1, E_2 all symmetry boundary conditions according to the loading direction were defined in Fig. 2 and Fig. 3, in detail. The axial loading was modeled by force and displacement. The elastic constants were obtained by using these two different loading applications such as: (i) mechanical loading (I): $P = 1$ N/node, (ii) displacement loading (II): $\delta = 1$ μm/node. The theoretical calculation of elastic constants was obtained using the rule of mixture equations given below

$$E_1 = E_f V_f + E_m (1 - V_f), \tag{1}$$

$$\nu_{12} = \nu_f V_f + \nu_m (1 - V_f), \tag{2}$$

$$\frac{1}{E_2} = \frac{V_f}{E_f} + \frac{(1 - V_f)}{E_m}. \tag{3}$$

Here, E_f, E_m — the Young modulus values for fiber and matrix, and ν_f, ν_m — the Poisson ratio values for fiber and matrix, and V_f — volume fraction for fiber, respectively.

TABLE I

Results of rule of mixture (ROM) and FEA, number of fibers nf, nodes nn and mesh elements nm used in FEA. E_i in [GPa].

V_f [%]	nf	E_1 (ROM)	E_2 (ROM)	E_1 (FEA)	E_2 (FEA)	SOLID187 nn	SOLID187 nm
10	9	1.40	1.14	1.38	1.23	66564	46805
17	16	1.64	1.21	1.47	1.25	66190	46519
27	25	1.98	1.32	1.72	1.40	37492	53326
40	36	2.43	1.51	2.44	1.47	38431	54662
54	49	2.91	1.79	2.96	1.95	58610	82513

3. Results and discussion

The numerical data obtained from the maximum stress and strain distributions were viewed on the counter nodal solutions from ANSYS. FEA applications and analytic approximations (ROM) gave similar elastic constants and they were presented on the curves in Figs. 3, 4 and 5. In case of the implementation of the symmetry boundary conditions on the rectangular and cubic prisms including the fibers which were embedded into the matrix material (RVE) unit-cell method was developed [9]. In the consideration of the mechanical P [N] and displacement δ [μm] based loadings, the obtained elastic constants were reached to different values that were mentioned in literature. According to these non-overlapping results, the approximate percentage relative error reached large scales (50%). In this research, by using the unit-cell method by cubic prisms, this error percentage was minimized. The mentioned problem aroused from usage of the rectangular prism while the stress distribution spread more easily drawn on the direction of the fibers and difference of the longitudinal elastic constants parallel to the fibers of the unit-cell was exceeded by the cubic geometry and the results of the two loading applications were overlapped (Fig. 6). The numerical and theoretical results were compared in Figs. 3–6. The approximate linear equation (E_1-trendline) was expressed in Eq. (4) and Fig. 3

$$E_1 = 0.0381V_f + 0.8629, \ R^2 = 0.9694. \quad (4)$$

The approximate quadratic equation obtained to present the E_2 distribution expressed in Eq. (5) and Fig. 4

$$E_2 = 0.0003\,(V_f)^2 - 0.0052\,(V_f) + 1.2609,$$
$$R^2 = 0.9859. \quad (5)$$

The approximate quartic and qubic equations (Eqs. (6)–(7))

$$\nu_{12} = -5 \times 10^{-7}\,(V_f)^4 + 6 \times 10^{-5}\,(V_f)^3$$
$$-0.0021\,(V_f)^2 + 0.0277\,(V_f) + 0.2548, \quad (6)$$

$$\nu_{23} = -1 \times 10^{-6}\,(V_f)^3 + 0.0003\,(V_f)^2 - 0.0244\,(V_f)$$
$$+0.6203 \quad (7)$$

were obtained by curve fitting numerical calculations to present the ν_{12} and ν_{23} distributions as seen in Fig. 5 (Eq. (3)).

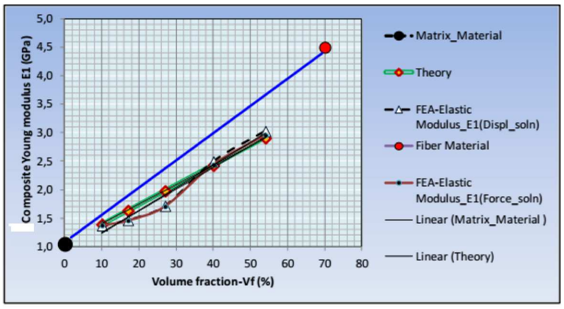

Fig. 3. Curves for the Young modulus E_1 values of the composite calculated along the fiber direction.

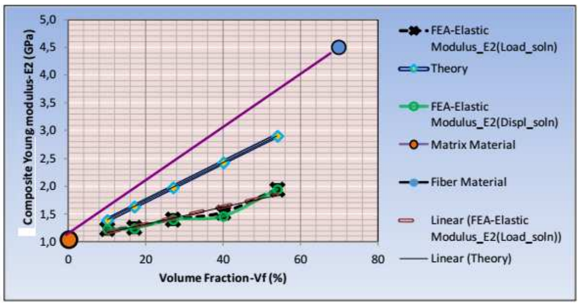

Fig. 4. Curves for the Young modulus E_2 values of the composite calculated perpendicular to the fiber direction.

The application of Z-axis directional mechanical (P) and displacement (δ) based loadings on "fiber composite polymer (PPE/PP) thermoplastic material" generated σ_z distributions as shown in Fig. 7a and b. The normal stress distribution generated on 9 fibers had higher values in case of displacement loading. The developing normal stresses at the tip points of the fibers were $(\sigma_z)_p = 0.348 \times 10^{-4}$ N/μm^2 and $(\sigma_z)_\delta = 0.105 \times 10^{-5}$ N/μm^2. The stress distribution results of the displacement (δ) based loading are shown in Fig. 7c. As it is shown in this figure, the calculated Z directional elongations over the free surface of the material were equal to $\delta_z = 0.78614$ μm whereas the equation for the inner sections

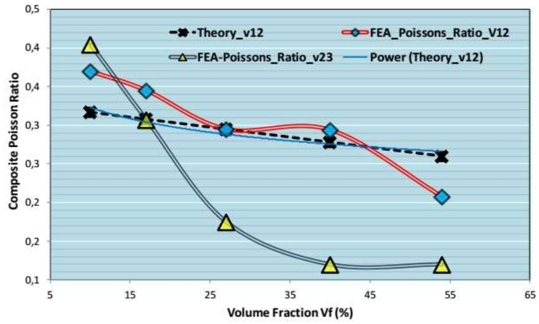

Fig. 5. Curves for the Poisson ratio values of the composite.

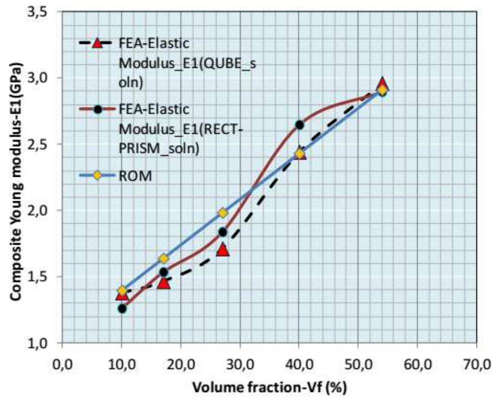

Fig. 6. Comparison of the FEA models.

was $\delta_z = 0.4297$ μm. This developing displacement (δ) distribution showed us an extremely large relative deformation area in the matrix section of the composite. The fiber and matrix material contained in the outer free surface of composite was stretched. Figure 7d and e illustrates the developing σ_z distribution on the 16 fibers and the matrix section in which the fibers embedded. The resulting stresses for the fibers and the matrix sections were equal to $(\sigma_z)_p = 0.193 \times 10^{-3}$ N /μm^2 and $(\sigma_z)_p = 0.3781 \times 10^{-3}$ N/μm^2, respectively. Mechanical loading generated σ_z distribution on 25 fibers as shown in Fig. 7f. Here, the calculated average stress was equal to $(\sigma_z)_p = 0.3847 \times 10^{-1}$ N/μm^2. Figure 7g presents the σ_z distribution developed on the matrix section (26 fibers, load type-(II)). In the other two FE fiber composite models there were 36 and 49 fibers (load type-(I)). The related results were shown in Fig. 7h and i. As shown in Fig. 7h, 36 fibers were approximately under the normal stress of $(\sigma_z)_p = 0.17305 \times 10^{-1}$ N/μm^2 and, as can be seen in Fig. 7i, the average stress distribution for the matrix section of the 49 fibers-matrix model was $(\sigma_z)_p = 0.282 \times 10^{-3}$ N/μm^2. Figure 7j and k illustrates the δ_x and σ_x distributions of the 9 fibers-matrix model (load type-(II)). The displacement loading was applied parallel to the x-axis. Figure 7l and m demonstrates the δ_x and ε_x distributions of 49 fiber-matrix model. The obtained average displacement and strain values were $\delta_z = 0.7748$ μm and $\varepsilon_z = 0.83 \times 10^{-2}$, respectively.

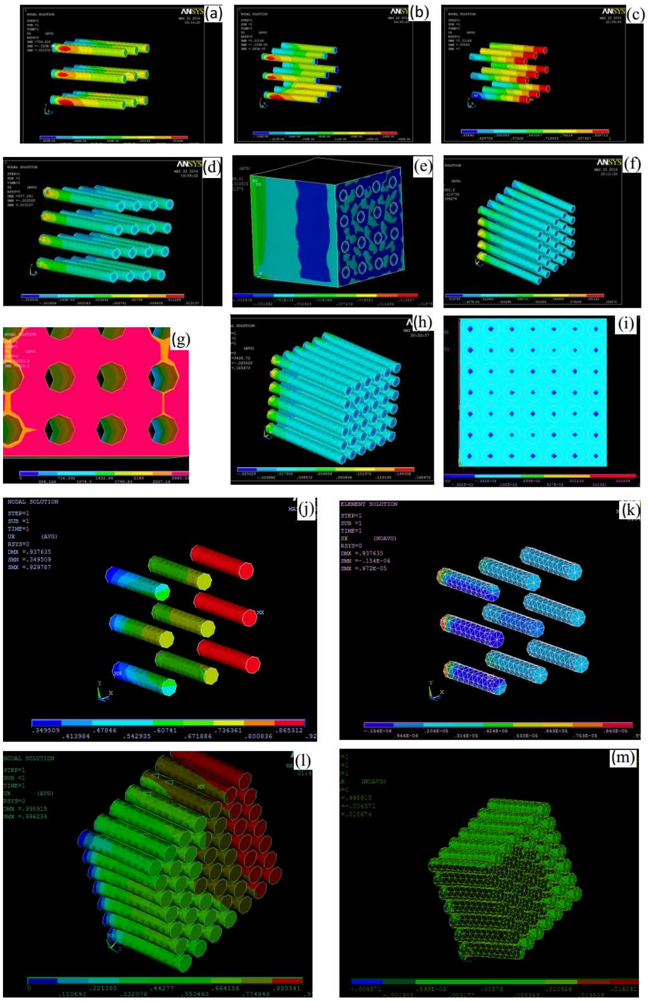

Fig. 7. (a) σ_z distribution on 9 fibers (load type-(I), fiber direction); (b) σ_z distribution on 9 fibers (load type-(II), fiber direction); (c) δ_z distribution on 9 fibers (load type-(II), fiber direction); (d) σ_z distribution on 16 fibers (load type-(I), fiber direction); (e) σ_z distribution on matrix surface and 16 fibers (load type-(I), fiber direction); (f) σ_z distribution on 25 fibers (load type-(I), fiber direction); (g) $\sigma_z$distribution on matrix (26 fibers, load type-(II), fiber direction); (h) σ_z distribution on 36 fibers (load type-(I), fiber direction); (i) σ_z distribution on the matrix and 49 fibers (load type-(I), fiber direction); (j) δ_x distribution on 9 fibers (load type-(II), loading perpendicular to fiber direction); (k) σ_x distribution on 9 fibers (load type-(II), loading perpendicular to fiber direction); (l) δ_x distribution on 49 fibers (load type-(II), loading perpendicular to fiber direction); (m) ε_x distribution on 49 fibers (load type-(II), loading perpendicular to fiber direction).

4. Conclusion

In this research, the main changes about the distribution of stresses on fibers and matrix by changing the fiber volume fraction and the loading direction were studied by using FEA (Fig. 7). According to the analyse results, when polymer type fiber and matrix elastic constants were used, the changing geometry, loading types and boundary conditions caused main changes in equivalent elastic constant values proportionally. The approptiate boundary conditions were applied in obtaining four elastic constants of the transversely isotropic PPE/PP material. The results obtained from 3D analysis for polymer microcomposite were summarized as below:

(1) A linear relationship between the first elastic constant E_1 and fiber volume fraction V_f [%] was detected [Fig. 3];

[2] A quadratic relationship between the second elastic constant E_2 and fiber volume fraction V_f [%] was detected [Fig. 4];

[3] Qubic and quartic relationships between the major and minor Poisson ratios ν_{12}, ν_{23} and fiber volume fraction V_f [%] were found [Fig. 5];

[4] For largest fiber volume fraction calculations, nearly constant the Poisson ratio value ν_{23} was obtained [Fig. 5],

[5] With fiber volume fraction V_f [%] increase, decreasing stress concentration in the fiber-matrix interface was detected [Fig. 7e]. This effect occurred according to the lack of sufficient space for the transmission from fiber to the matrix due to the high fiber content V_f [54%].

Acknowledgments

Thanks for the great supports of FIGES and Gazi University BAP project under grant No. 06/2011-57. This study was performed in Gazi University, Mechanical Engineering Department, Ankara, Turkey.

References

[1] F.C. Campbell, *Structural Composite Materials*, ASM International, 2010.

[2] P. Bhaskar, M.R. Haseebuddin, *Adv. Mater. Phys. Chem.* **2**, 23 (2012).

[3] E. Günay, Z. Ece, M.A. Esi, *Mech. Compos. Mater.* **44**, 349 (2008).

[4] H.L. Cox, *Brit. J. Appl. Phys.* **3**, 72 (1952).

[5] S. Houshyar, R.A. Shanks, A. Hodzic, *Express Polym. Lett.* **3**, 2 (2009).

[6] C.T. Sun, R.S. Vaidya, *Compos. Sci. Technol.* **56**, 171 (1996).

[7] K. Hbaieb, Q.X. Wang, Y.H.J. Chia, B. Cotterell, *Polymer* **48**, 901 (2007).

[8] B. Jiang, C. Liu, C. Zhang, R. Liang, B. Wang, *Composites Part B* **40**, 212 (2009).

[9] I. Alfonso, V.R. Iglesias, I.A. Figueroa, *Revistamateria* **20**, 293 (2015).

[10] S. Houshyar, R.A. Shanks, A. Hodzic, *J. Appl. Polym. Sci.* 96, 2260 (2005).

[11] A.G. Facca, M.T. Kortschot, N. Yan, *Composites Part A* **37**, 1660 (2006).

[12] M. Klasztorny, P. Konderla, R. Piekarski, *Mech. Compos. Mater.* **45**, 77 (2009).